

Designing Several Types of Oscillation-Less and High-Resolution Hybrid Schemes on Block-Structured Grids

Zhenhua Jiang*, Chao Yan*, Jian Yu and Boxi Lin

College of Aeronautics Science and Engineering, Beijing University of Aeronautics and Astronautics, Beijing 100191, P.R. China.

Communicated by Kun Xu

Received 20 December 2015; Accepted (in revised version) 6 August 2016

Abstract. An idea of designing oscillation-less and high-resolution hybrid schemes is proposed and several types of hybrid schemes based on this idea are presented on block-structured grids. The general framework, for designing various types of hybrid schemes, is established using a Multi-dimensional Optimal Order Detection (MOOD) method proposed by Clain, Diot and Loubère [1]. The methodology utilizes low dissipation or dispersion but less robust schemes to update the solution and then implements robust and high resolution schemes to deal with problematic situations. A wide range of computational methods including central scheme, MUSCL scheme, linear upwind scheme and Weighted Essentially Non Oscillatory (WENO) scheme have been applied in the current hybrid schemes framework. Detailed numerical studies on classical test cases for the Euler system are performed, addressing the issues of the resolution and non-oscillatory property around the discontinuities.

AMS subject classifications: 65Y20, 65M08

Key words: Hybrid schemes, oscillation-less, high resolution, MOOD, finite volume.

1 Introduction

When solving nonlinear hyperbolic conservation laws, how to achieve both the high resolution and the non-oscillatory property around the discontinuities may remain one of the most important questions. It is well known that interpolations across discontinuities tend to generate spurious oscillations that can ultimately lead to a failure of the computation. And there has been an abundance of work to deal with the conflict between keeping the high accuracy of the solutions and stabilizing the computation. Among all

*Corresponding author. *Email addresses:* zhenhua122122@163.com (Z. Jiang), yanchao@buaa.edu.cn (C. Yan), yuj@buaa.edu.cn (J. Yu), boxi.lin@163.com (B. Lin)

popular techniques we can cite MUSCL (monotone upstream scheme for conservation law) methods [2], weighted essentially non-oscillatory (WENO) schemes [3, 4] and central schemes [5].

MUSCL method was developed by van Leer [2] to construct high resolution total variation diminishing (TVD) schemes for solving hyperbolic conservation laws. Due to the ability to preserve stability, monotonicity as well as greater order of accuracy, MUSCL methods have become a standard widely used in today's commercial codes. For flows with strong shock waves, the use of limiters becomes necessary for preventing solution overshoots that may compromise accuracy and stability. However, it is well-known that no classical limiter has been found to work well for all problems. Indeed, some efficiently capture discontinuities but bring about some squaring effect on smoother waves, whereas other ones are accurate on smooth waves but more dissipative for sharp gradients [6]. WENO schemes utilize an adaptive stencil based on the local smoothness of the numerical solution to achieve high accuracy while avoiding oscillations near discontinuities. Higher-order WENO schemes have been constructed [7] for reducing numerical diffusion and their superior accuracy over low-order schemes for smooth flows has been demonstrated. However there are also some drawbacks of high-order WENO schemes, such as suboptimal convergence for a class of smooth solutions as well as excessive dissipation across discontinuities. For example, a characteristic-based MUSCL scheme shows better resolution for the contact discontinuity than a fifth-order WENO scheme [8]. As an alternate strategy, central schemes [5] achieve nonlinear stability through the use of artificial-dissipation models. The major difficulty in central schemes is making sure that a sufficient amount of stabilizing diffusion is added wherever it is needed to ensure stability, while in the rest of the computational domain the diffusion must be small enough not to affect the high accuracy of the scheme there. However the central schemes usually contain the artificial coefficients that are both mesh- and problem-dependent. Worse yet, there is no any guide line regarding the choice of these artificial coefficients.

A natural idea is then to develop schemes that combine the advantages of different schemes described above and avoid the disadvantages inherent in each method. Such so-called hybrid schemes have been constructed in the literature [9–14] and most of the researches utilize schemes either with spectral-like resolution [9–11] or schemes with a high order of accuracy and high efficiency in smooth regions [12–14] and then hybridize the ENO/WENO schemes to handle discontinuities. More importantly, an important component of all present hybrid schemes is using an indicator to automatically identify the discontinuity of the solution where the shock-capturing schemes can be applied. The Ref. [14] has systematically investigated a wide range of such indicators, although efficient and reliable indicators are still warranted today. Inspired by the previous work, the objective of this paper is to establish a general framework for designing various types of hybrid schemes with emphasis on achieving the high resolution and oscillation-free property around discontinuities. The novelty is to construct hybrid schemes based on a new concept of MOOD approach, which was originally proposed in [1] and further extended in the following studies [15–18]. Based on the MOOD concept, the resulting approach

does not use any indicator in designing hybrid schemes. We first utilize low dissipation or dispersion but less robust schemes to update the solution and then implement robust and high resolution schemes to deal with problematic situations. A wide range of computational methods including central scheme, MUSCL scheme, linear upwind scheme and WENO scheme have been applied in the current hybrid schemes framework. Also different from the published methods, the present work employs a carefully designed TVD scheme to deal with problematic solutions, since this scheme has shown the high resolution on the discontinuity based on our previous research [8, 19].

The rest of the paper is organized as follows. Section 2 briefly introduces the governing equation and the finite volume (FV) formulation applied in the work. Section 3 describes the details of designing several types of hybrid schemes in the developed framework. Numerical tests are carried out in Section 4 and some conclusions are drawn in Section 5.

2 The governing equation and the finite volume discretization

2.1 Governing equations

Let us now consider the nonlinear system of hyperbolic conservation laws in multiple space dimensions of the form

$$\frac{\partial Q}{\partial t} + \frac{\partial F(Q)}{\partial x} + \frac{\partial G(Q)}{\partial y} + \frac{\partial H(Q)}{\partial z} = 0, \quad (2.1)$$

where Q are conservative variables, $F(Q)$, $G(Q)$ and $H(Q)$ are flux vectors depending on state Q in Cartesian coordinates, and t means time.

In this paper, we solve the system of equations (2.1) by using the finite volume method on multi-block structured grids. Firstly, the computational domain is discretized by a grid of conforming elements $\Omega_{i,j,k}$. The subscript " i,j,k " is used to indicate the numbering of the cell in the 3D structured grids.

The numerical solution of Eq. (2.1) for the conservative variables Q is represented within each cell $\Omega_{i,j,k}$ by cell average $\bar{Q}_{i,j,k}$ defined as

$$\bar{Q}_{i,j,k} = \frac{1}{V} \int_{\Omega_{i,j,k}} Q(x,y,z,t) d\Omega, \quad (2.2)$$

where V is the cell volume. Then Eq. (2.1) is integrated over $\Omega_{i,j,k}$ to obtain

$$\frac{d\bar{Q}_{i,j,k}}{dt} + \frac{1}{V} \int_{\partial\Omega} \vec{F} \cdot \vec{n} ds = 0, \quad (2.3)$$

where $\vec{F} = (F(Q), G(Q), H(Q))$ is inviscid flux tensor and \vec{n} is the outward unit normal vector to the boundary $\partial\Omega$ of the cell $\Omega_{i,j,k}$. Then, the flux $\vec{F} \cdot \vec{n}$ is replaced by a numerical

approximation of convective flux at the interface as

$$\vec{F} \cdot \vec{n} = \hat{F}(Q_L, Q_R, \vec{n}), \quad (2.4)$$

where Q_L and Q_R are the solution states on the left and right sides of the interface. Depending on the way the convective flux of the interface is approximated, the class of FV schemes can be split into two subclasses: upwind schemes and central schemes.

2.2 FV discretization: upwind schemes and central schemes

Upwind schemes, in their most popular form, are usually implemented in two stages:

1. A reconstruction stage which obtains a representation of the solution surface given cell-averaged data;
2. The reconstructed variables on either side of the interface are interpreted for approximate Riemann solvers.

For the hybrid schemes addressed here, the issues are independent of the choice of the Riemann solvers and an approximate Riemann solver of Roe [20] is employed in this work. As for the reconstruction stage, monotonicity principles are invoked to capture the discontinuities without causing spurious oscillations. The procedures of the reconstruction for present work include the linear reconstruction (the 3rd-order and the 5th-order accuracy), the MUSCL method (either variable-based or characteristic-based), and the variable-based WENO method, which will be described in detail in Subsections 3.2-3.4.

As an alternate strategy, central schemes treat discontinuities as smooth solutions but with large gradient. In order to do so, numerical dissipation models are required in the central scheme. And the convective flux \hat{F} in Eq. (2.4) can be decomposed into the pure central part and the artificial dissipation

$$\hat{F} = F_c - F_{ad}. \quad (2.5)$$

As mentioned earlier, artificial dissipation models are detrimental to the performance of central schemes. And this work will prove that the designed hybrid schemes based on the central schemes can be much more reliable and accurate compared with the original methods.

After the FV discretization of the governing equation by using either upwind or central schemes, the resulting system of ordinary differential equations (2.3) is discretized in time by a third-order version of TVD Runge-Kutta method [4].

3 Several types of oscillation-less and high-resolution hybrid schemes

The approach in this section is to describe first the general framework for designing hybrid schemes, and then move on to present several different types of hybrid schemes that

have been designed to achieve both the high resolution and the oscillation-less property around discontinuities.

3.1 General framework for designing hybrid schemes based on the MOOD concept

Most of the aforementioned hybrid schemes have a common feature that an indicator is relied on to identify the locations where the shock-capturing schemes are needed. While vast literatures on designing such indicators exist, according to the exploration in [14] there is no universally better performing method for every problem. Recently, the Ref. [18] has reviewed these indicators or limiters in the framework of discontinuous Galerkin (DG) and classified them as a priori detecting, which means such indicators as well as limiters rely on the fact that spurious numerical oscillations can be detected and corrected in the discrete solution by looking at only one time step and usually without using the PDE.

On the contrary, the concept of MOOD approach, originally proposed in [1] and further extended in the following studies [15–18], is known as an a posteriori detection approach. By looking at two different time levels and recomputing the solution, the detection criterion has been proven to be able to dissipate numerical oscillations and ensure stability. Therefore this work has proposed to construct hybrid schemes based on this new MOOD approach.

Now we catalogue the details of the hybrid schemes which are built on the MOOD approach. We consider the simple case of each explicit sub-step discretization of the TVD RungeKutta method which corresponds to a convex combination of several explicit steps.

We assume that Q^n is an approximation of conservative variables Q at time t^n , and the goal is to build the solution Q^{n+1} at time $t^{n+1} = t^n + \Delta t$. To this end, the hybrid schemes proceed as follows:

Firstly, we utilize low dissipation or dispersion but less robust schemes to compute a solution using the finite volume discretization (2.4), also known as obtaining the candidate solution $Q^*(t^{n+1})$ by

$$\frac{dQ^*}{dt} + \mathbf{Rhs}_{original}(Q^n) = 0, \quad (3.1)$$

where $\mathbf{Rhs}_{original}$ denotes the residual term obtained by the original scheme that is low dissipation or dispersion but less robust as mentioned earlier. Note that this step in the approaches of hybrid schemes is different from the procedure proposed in the references of MOOD schemes [1, 18], where an unlimited high order scheme is used to compute the candidate solution Q^* . Currently, we design hybrid schemes that still hybridize two types of schemes, therefore the techniques adopted here may not be the same as the full successive order decrementing loop adopted in the original MOOD approaches.

Secondly, once the candidate solution Q^* is obtained, the detection criteria of physical admissibility and numerical admissibility are immediately applied. The physical admissibility restricts that physically relevant quantity, such as the density ρ and the pressure

p for the Euler equations, must satisfy the positivity constraint. For the FV method, here we apply physical admissibility for cell average over each cell as

$$\bar{\rho}(\mathbf{Q}^*) > 0, \quad \bar{p}(\mathbf{Q}^*) > 0, \tag{3.2}$$

which is simple because no reconstructed values at quadrature points have to be considered.

Meantime the numerical admissibility restricts that the candidate solution must satisfy the discrete maximum principle (DMP). Like the Ref. [18], we use the relaxed version of a discrete maximum principle

$$\min(\bar{\mathbf{Q}}_m^n(t^n)) - \delta < \bar{\mathbf{Q}}_{ijk}^*(t^{n+1}) < \max(\bar{\mathbf{Q}}_m^n(t^n)) + \delta, \quad m \in \bar{v}_{ijk}, \tag{3.3}$$

where \bar{v}_{ijk} is a set containing cell I_{ijk} together with its Voronoi neighbor cells that share a common node with cell I_{ijk} . Again for the FV method, numerical admissibility has been applied for cell average over each cell. Also according to [18], the quantity δ is used to relax the strict maximum principle and is obtained as

$$\delta = \max\left(10^{-4}, 10^{-3} \cdot (\max(\bar{\mathbf{Q}}_m^n) - \min(\bar{\mathbf{Q}}_m^n))\right), \quad m \in \bar{v}_{ijk}. \tag{3.4}$$

After applying the physical admissibility and numerical admissibility detection, a cell is marked as one of the three types of cells: the original cell, the recomputed cell or the reassembled cell. To be specific, if the candidate solution of the cell fails to fulfill either Eq. (3.2) or Eq. (3.3), the cell is marked to be recomputed. Then for those cells that share a common face with the recomputed cells and meantime fulfill the detection criteria in both the Eq. (3.2) and the Eq. (3.3), they are marked to be reassembled. At last, the rest of the cells are marked as the original cell.

Thirdly, the solution \mathbf{Q}^{n+1} can be finally obtained by different numerical schemes in accordance with the cell type marked by the procedure described above. It is evident that for the "original" cells, $\mathbf{Q}^{n+1} = \mathbf{Q}^*$ that is directly obtained from the Eq. (3.1). It is more challenging to deal with problematic solutions for the "recomputed" cells, because it requires a shock-capturing scheme that is robust, oscillation-free therefore to handle problematic situations and meantime has high accuracy and/or high resolution characteristics therefore to capture fine flow structures. Once the shock-capturing scheme is determined, the solution \mathbf{Q}^{n+1} for the "recomputed" cells is recomputed from the Eq. (3.5) using the solution at time t^n . At last, the residuals of the "reassembled" cells only need to reassemble: for those faces connected to the "recomputed" cells the recomputed convective flux of the interface is chosen, otherwise the original convective flux of the interface is chosen. Thus the solution \mathbf{Q}^{n+1} for the "reassembled" cells is obtained from the Eq. (3.6) using the reassembled residual term

$$\frac{d\mathbf{Q}^{n+1}}{dt} + \mathbf{Rhs}_{recomput}(\mathbf{Q}^n) = 0, \tag{3.5}$$

$$\frac{d\mathbf{Q}^{n+1}}{dt} + \mathbf{Rhs}_{reassemble}(\mathbf{Q}^n) = 0. \tag{3.6}$$

Remark 3.1. The idea behind the present framework for designing hybrid schemes is by taking advantage of the concept of MOOD method, the construction of hybrid schemes is completely turned into the construction of different numerical flux for the interface between the cells. As can be seen, the solution is obtained either from Eq. (3.1) or from Eq. (3.5) or Eq. (3.6), where the only difference is the different evolution procedures for the interface flux. As a result, theoretically any numerical scheme can be applied in the current hybrid schemes framework. For instance, this work has designed hybrid schemes that combine the central scheme and the upwind scheme, two very different numerical schemes in the FV discretization, and has proved its superior performance owing to this combination.

Remark 3.2. There are three major differences between the present hybrid schemes and the original MOOD methodology [1]. First, one or both of the building blocks is/are shock capturing scheme(s) with a priori limiter instead of unlimited MUSCL methods in the original algorithm. Secondly, the original MOOD scenario uses full successive order decrementing loop while the method in this paper only hybridizes two types of schemes, which therefore uses only one loop. In the original MOOD scenario, the DMP is of important concern. Although the adopted characteristic-based MUSCL scheme is a robust shock-capturing scheme, we admit that there is still no guarantee in attaining the DMP property like the original MOOD with substantial theoretical analysis. Thirdly, the present method adopts a relaxed version of DMP, as can be seen from Eq. (3.3), where δ is to relax the strict maximum principle in order to allow some small overshoots and undershoots [18]. In authors opinion this may also have caused influence on the DMP property of the present method because some cells can be marked as the original cell though they may violate the strict maximum principle.

3.2 Shock-capturing schemes: characteristic-based MUSCL scheme

As mentioned in previous subsection, it is more challenging to deal with problematic solutions for the "recomputed" cells. The basic guild line is choosing schemes that are robust, oscillation-free and meantime with high accuracy and/or high resolution characteristics. Although most of hybrid schemes in the literature [9–14] hybridize the ENO/WENO schemes to do the job, the present work employs a characteristic-based MUSCL scheme based on our previous research [8, 19] on the comparison of these two types of schemes.

MUSCL interpolation can be written as

$$\begin{aligned} Q_{i+1/2}^L &= \bar{Q}_i + \frac{1}{2} \Delta Q_i, \\ Q_{i+1/2}^R &= \bar{Q}_{i+1} - \frac{1}{2} \Delta Q_{i+1}, \end{aligned} \quad (3.7)$$

where $Q_{i+1/2}^L$ and $Q_{i+1/2}^R$ are left and right variables at interface, and Q_i is the variable slope in cell i .

Most high resolution schemes are derived on scalar conservation laws first, and then extended to systems of equations, which bring on the issue of working variables. There are a number of options available, including conservative, primitive and characteristic variables. According to Ref. [21], the choice of working variables can have a great impact on computation results. Characteristic decomposition is chosen here to suppress spurious oscillations. First, conservative variables are projected to characteristic space by

$$\mathbf{W}_j = \mathbf{L}_i \mathbf{Q}_j, \quad j = i-1, i, i+1. \quad (3.8)$$

Then, the slope of characteristic variables in cell i is determined as

$$\Delta \mathbf{W}_i = \varphi(\Delta \mathbf{W}_{i-1/2}, \Delta \mathbf{W}_{i+1/2}), \quad (3.9)$$

where φ represents limiter, and $\Delta \mathbf{W}_{i+1/2} = \mathbf{W}_{i+1} - \mathbf{W}_i$.

Finally, we have

$$\Delta \mathbf{Q}_i = \mathbf{R}_i \Delta \mathbf{W}_i, \quad (3.10)$$

\mathbf{L}_i and \mathbf{R}_i are the left and right eigenvector matrices of the Jacobian matrix \mathbf{A}_i of $\mathbf{F}(\mathbf{Q})$.

There are various ways for computing \mathbf{A}_i . In this paper, we adopt a local linearization method [19], which ensures that \mathbf{L}_i and \mathbf{R}_i are strictly conjugate inverse matrices and numerical errors from the transformation procedures can be effectively reduced. The choice of limiter φ in Eq. (3.9) is a crucial part. It is known that two types of waves, convective (or linear) waves and acoustic waves are differentiated when one performs the projection of the conservative variables into characteristic space. With the characteristic-based MUSCL scheme, the most compressive superbee limiter is used on the characteristic variables that are connected to convective (or linear) waves to obtain high resolution for contact discontinuities, while the double minmod limiter is used on the characteristic variables that are connected to acoustic waves to enhance stability. This MUSCL scheme is able to avoid the over compression of superbee limiter to contact discontinuities, as well as to maintain good robustness with relatively low computation cost.

3.3 Hybrid schemes using the MUSCL and WENO method

When constructing hybrid schemes, one usually looks for higher order methods to achieve more accurate simulation for various flow features. However today the second-order MUSCL methods are widely-used standard in industrial finite volume codes, hence it is important to construct a hybrid scheme composed of two MUSCL schemes and meantime it is important to prove the resulting hybridization can significantly improve the performance of standard second-order method.

As formulated in Eq. (3.7), an important aspect of MUSCL scheme is limiters that obtain the variable slope $\Delta \mathbf{Q}$. And it is well-known that superbee limiter is the least dissipative and also least stable limiter in the classical limiters. Furthermore different from characteristic-based MUSCL scheme, which is carefully designed for shock-capturing,

the most popular technique adopted in classical limiters is based on primitive variables. Therefore our first hybrid scheme is the hybridization of MUSCL scheme using primitive-variable based superbee limiter and the shocking-capturing scheme developed in Subsection 3.2.

The second hybrid scheme involves a WENO-like scheme. And this implementation of WENO is quite different from the traditional high order method for FV computation such as the work in [26, 27]. First, for two- and three-dimension problems there are essentially two ways for the reconstruction: genuine multidimensional reconstruction and dimension-by-dimension reconstruction. The genuine multidimensional reconstruction considers all cells in the multidimensional stencil simultaneously to build up a reconstruction polynomial, whereas dimension-by-dimension reconstruction consists of a number of one-dimensional reconstruction sweeps. The dimension-by-dimension reconstruction is much simpler and less computationally expensive than the genuine multidimensional one; this is especially so in three space dimensions [26]. Therefore, in this work we use dimension-by-dimension reconstruction. Besides, regarding quadrature points, current implementation chooses the strategy in [22], where the WENO reconstruction is only used to increase the spatial order of primitive variable interpolation to cell interface in a form analogous to MUSCL scheme, this is also different from traditional method [15, 16, 26, 27] where the Gaussian integration points are usually invoked. The resulting WENO scheme is variable-based and is applied component by component instead of the characteristic decomposition. The WENO-like implementation in the paper should only have numerical benefits by borrowing the form of the WENO5 scheme, but have the second- other than the fifth-order theoretically. And as a result only a small amount of additional cost is gained though the characteristic of the original WENO method cannot be completely realized. And in authors opinion, it may be both the implementation strategy (in particular without the characteristic decomposition) and the quadrature strategy that have caused oscillatory results with present WENO method, especially when one considers more demanding test problems or when the order of accuracy of reconstruction is high.

Taking $Q_{i+1/2}^L$ as an example, the WENO interpolation is given by

$$\begin{aligned}
 Q_{i+1/2}^L &= \omega_0 q_0 + \omega_1 q_1 + \omega_2 q_2, \\
 q_0 &= \frac{1}{3} \bar{Q}_{i-2} - \frac{7}{6} \bar{Q}_{i-1} + \frac{11}{6} \bar{Q}_i, \\
 q_1 &= -\frac{1}{6} \bar{Q}_{i-1} + \frac{5}{6} \bar{Q}_i + \frac{1}{3} \bar{Q}_{i+1}, \\
 q_2 &= \frac{1}{3} \bar{Q}_i + \frac{5}{6} \bar{Q}_{i+1} - \frac{1}{6} \bar{Q}_{i+2},
 \end{aligned} \tag{3.11}$$

where q_0 , q_1 and q_2 represent three third order stencils, which are combined with nonlinear weights ω_k to form a fifth order interpolation. The expressions of nonlinear weights

ω_k are given by

$$\omega_k = \frac{\alpha_k}{\alpha_0 + \alpha_1 + \alpha_2}, \quad (3.12)$$

$$\alpha_k = \frac{C_k}{(\varepsilon + IS_k)^2}, \quad k=0,1,2, \quad C_0=0.1, \quad C_1=0.6, \quad C_2=0.3, \quad (3.13)$$

where $\varepsilon = 10^{-6}$ and C_k are optimal weights yielding a truly high-order algorithm in the smooth region.

The two hybrid schemes in this subsection have a common feature: the scheme used to obtain the candidate solution is the upwind scheme with the shock-capturing capability. In the current framework, we develop this type of hybrid schemes to demonstrate the capability of the hybridization in simultaneously retaining the advantage and remedying the defect of the original method. In particular we will show the hybrid schemes can gain the high resolution and non-oscillatory property around discontinuities.

3.4 Hybrid schemes using linear reconstruction method

The second type of hybridization is to combine high order linear reconstruction method with the present shock-capturing scheme, which is similar to the work in [14], although the work in [14] has been performed in the finite difference framework and has used 5th-order WENO method with priori detecting indicators.

In the FV discretization, the linear reconstruction is applied in a form very analogous to the WENO scheme. For instance the 5th-order linear interpolation can be written as:

$$\mathbf{Q}_{i+1/2}^L = C_0 \mathbf{q}_0 + C_1 \mathbf{q}_1 + C_2 \mathbf{q}_2, \quad (3.14)$$

where \mathbf{q}_0 , \mathbf{q}_1 and \mathbf{q}_2 are three third order stencils from Eq. (3.11) and C_0 , C_1 and C_2 are optimal weights from Eq. (3.11). Similarly we also adopt the 3rd-order linear reconstruction in this work as follows:

$$\begin{aligned} \mathbf{Q}_{i+1/2}^L &= C_0 \mathbf{q}_0 + C_1 \mathbf{q}_1, \quad C_0 = \frac{1}{3}, \quad C_1 = \frac{2}{3}, \\ \mathbf{q}_0 &= -0.5 \bar{\mathbf{Q}}_{i-1} + 1.5 \bar{\mathbf{Q}}_i, \\ \mathbf{q}_1 &= 0.5 \bar{\mathbf{Q}}_i + 0.5 \bar{\mathbf{Q}}_{i+1}, \end{aligned} \quad (3.15)$$

where \mathbf{q}_0 and \mathbf{q}_1 are two second order stencils and C_0 and C_1 are optimal weights for the 3rd-order linear reconstruction.

The reconstructions in Eq. (3.14)-(3.15) are upwind linear reconstructions and hence the resulting schemes are denoted as UP3 and UP5 schemes in the paper. Note that there are other choices also applicable in the current framework including a low phase error fourth-order formula

$$\mathbf{Q}_{i+1/2}^L = (9\mathbf{Q}_{j-2} - 56\mathbf{Q}_{j-1} + 194\mathbf{Q}_j + 104\mathbf{Q}_{j+1} - 11\mathbf{Q}_{j+2})/240$$

or even an implicit formula

$$\left(3Q_{i-1/2}^L + 6Q_{i+1/2}^L + Q_{i+3/2}^L\right) / 10 = \left(Q_{j-1} + 19Q_j + 10Q_{j+1}\right) / 30.$$

3.5 Hybrid schemes using central schemes

The previously designed two types of hybrid schemes are the combination of two upwind schemes and this subsection will present the third type of hybrid scheme that includes both the central scheme and the upwind scheme.

As formulated in Eq. (2.5), the convective flux \hat{F} of the central schemes is decomposed into the pure central part and the artificial dissipation. The development of artificial dissipation term F_{ad} has drawn most attention because it is detrimental to the performances of central schemes. However here we just choose the basic algorithm developed in the seminal work of Jameson et al. [5]. This artificial dissipation term F_{ad} contains a blending of the second-difference and fourth-difference terms and is expressed as

$$F_{ad,i+1/2} = \lambda_{i+1/2} \left(\varepsilon_{i+1/2}^{(2)} \delta Q - \varepsilon_{i+1/2}^{(4)} \delta^3 Q \right)_{i+1/2}, \quad (3.16)$$

where $\delta Q_{i+1/2} = Q_{i+1} - Q_i$, $\delta^3 Q_{i+1/2} = Q_{i+2} - 3Q_{i+1} + 3Q_i - Q_{i-1}$ and λ is the spectral radii of the Jacobian matrix.

In the models, the contributions from the second-difference and fourth-difference are controlled by two parameters, $\varepsilon^{(2)}$ and $\varepsilon^{(4)}$, respectively. They are computed as

$$\begin{aligned} \varepsilon_{i+1/2}^{(2)} &= k^{(2)} \max(v_i, v_{i+1}), \\ \varepsilon_{i+1/2}^{(4)} &= \max \left[0, (k^{(4)} - \varepsilon_{i+1/2}^{(2)}) \right], \end{aligned} \quad (3.17)$$

where ε is a shock sensor in the form of

$$v_i = \frac{|p_{i+1} - 2p_i + p_{i-1}|}{p_{i+1} + 2p_i + p_{i-1}}. \quad (3.18)$$

As can be seen in Eq. (3.17), there are two user-specified constants $k^{(2)}$ and $k^{(4)}$. And the central schemes can work well only when this set of parameters are well-tuned. However there is no any guide line regarding the choice of these parameters. In order to overcome this difficulty in central schemes, the third type of hybrid scheme is suggested here. Our method is to implement central schemes with a low dissipation/dispersion to obtain candidate solution and then use characteristic-based MUSCL scheme to handle the problematic solutions. Since the artificial-dissipation models are no longer responsible for the capture of discontinuous solutions, the burden on the choice of artificial coefficients can be much alleviated and even can be completely removed. In fact, current work has fixed $k^{(2)} = 0.05$ and $k^{(4)} = 0.008$ for all test cases listed in Section 4 when using the third type of hybrid scheme.

3.6 Further remark on the designed hybrid schemes

Remark 3.3. The general framework for hybrid schemes is built on the concept of MOOD approach. By reformulating the approach as the hybridization of different numerical flux of the interface, any numerical scheme, with either low dissipation/dispersion characteristic or good shock-capturing ability, can be applied in the current framework. No prior detecting indicators are needed for the resulting approach. And moreover, compared to previous studies [9-14] that mainly concentrates on high order schemes, this work also includes the second-order schemes, such as the MUSCL scheme and the central scheme, with emphasis on achieving significant performance improvement over the original method.

Remark 3.4. Though the present method is performed on block-structured grids, the basic idea and the general framework for designing hybrid schemes are not restricted to the type of grids. We develop hybrid schemes on structured grids because some schemes, for example high order WENO and linear reconstruction schemes, are more easily constructed on structured grids.

Remark 3.5. The emphasis of the present implementation has been mainly focused on achieving significant performance improvement over the original FV schemes. And the mathematical property of current method will depend on the property of two specific schemes that are adopted in the hybridization. Take hybrid WENO for example, it can achieve essentially non-oscillatory property since the solutions are obtained either by the WENO scheme or a less oscillatory shock-capturing scheme. However since the basic idea for our proposed hybrid schemes is taking full advantage of a low dissipation/dispersion characteristic from the original methods and a good shock-capturing ability from the shock-capturing methods (i.e. the characteristic-based MUSCL scheme in this work), therefore for all designed hybrid schemes, the current implementation will possess the property of preserving high accuracy in the smooth regions of the solution and simultaneously achieving oscillation-less, high resolution characteristics around discontinuities.

4 Numerical results

In this section, the accuracy test for the hybrid schemes is carried out first, and then some typical numerical examples for Euler system are presented to demonstrate the performance of the designed hybrid schemes. As mentioned in Subsection 3.1, a third order TVD RK scheme [4] is applied as the time stepping scheme and a CFL number 0.3 is used for all considered cases.

4.1 Accuracy test

We first test the capability of the method to achieve the desired accuracy for the Euler equations. The exact solution is given by $\rho = 1 + 0.2\sin\theta$, $u = 1$, $v = 1$, $p = 1$, $\theta = x + y - t$.

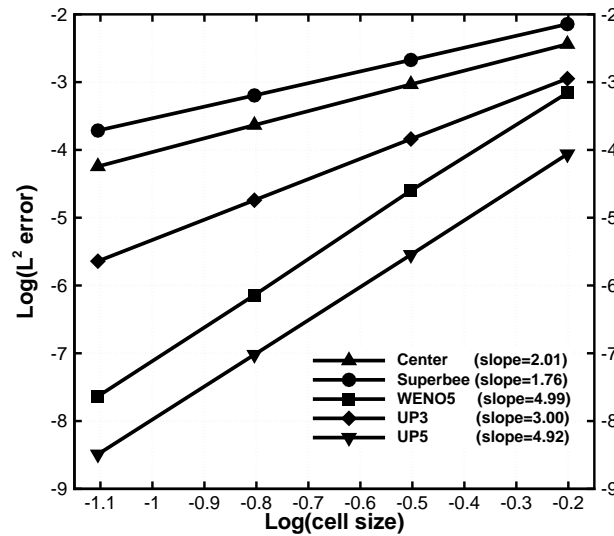


Figure 1: Convergence rates of the designed several types of hybrid schemes.

The convergence test is conducted on the spatial domain $[-\pi, \pi] \times [-\pi, \pi]$ from the time $T=0$ to $T=0.2$. The meshes used in this study are single block meshes, for the coarsest case with cell size $h = \pi/5$. The errors presented are those of the cell averages of density.

Fig. 1 provides the comparison on convergence rates of the hybrid schemes based on the superbee, WENO, UP3, UP5 and central schemes, respectively. It can be seen that the hybrid schemes give the desired convergence rates, demonstrating that for the smooth solution problem the designed order accuracy can be achieved using the current hybrid schemes.

4.2 Sod problem

The hybrid schemes are applied to one-dimensional shock tube problem. The computational domain contains 101 vertices in the x -direction. The initial conditions are

$$(\rho, u, p) = \begin{cases} (1, 0, 1), & x < 0, \\ (0.125, 0, 0.1), & x \geq 0. \end{cases} \quad (4.1)$$

In order to examine the capability of the hybrid methods, for this and the following cases, we compare the first and third type of hybrid schemes with their corresponding original schemes, while for the second type of hybrid schemes we compare them with the current WENO-like scheme without hybridization. And when the original central schemes are applied, two sets of parameter: $k^{(2)}=0.05, k^{(4)}=0.008$ and $k^{(2)}=0.3, k^{(4)}=0.03$ are used.

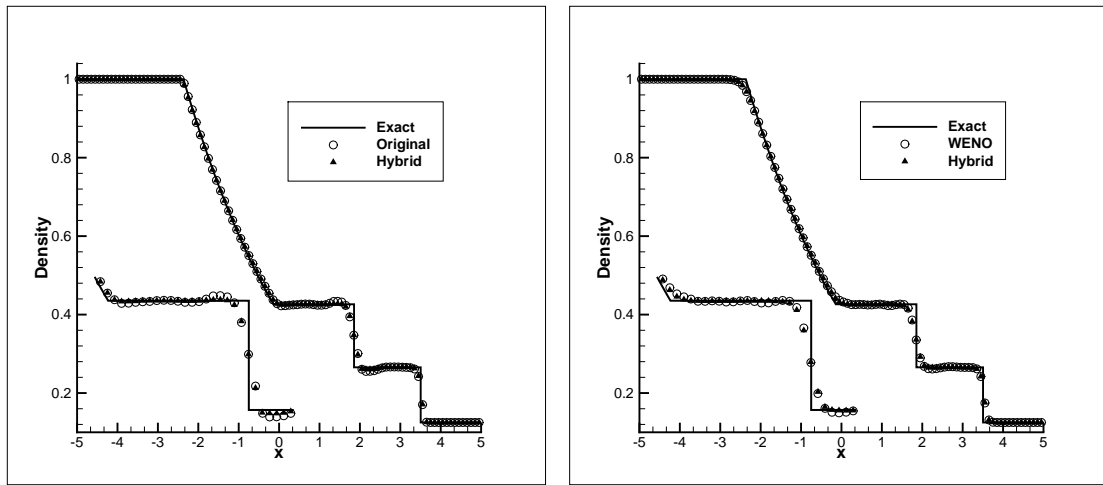


Figure 2: Density profiles of solutions to the Sod problem obtained by the first type of schemes: left: superbee; right: WENO-like.

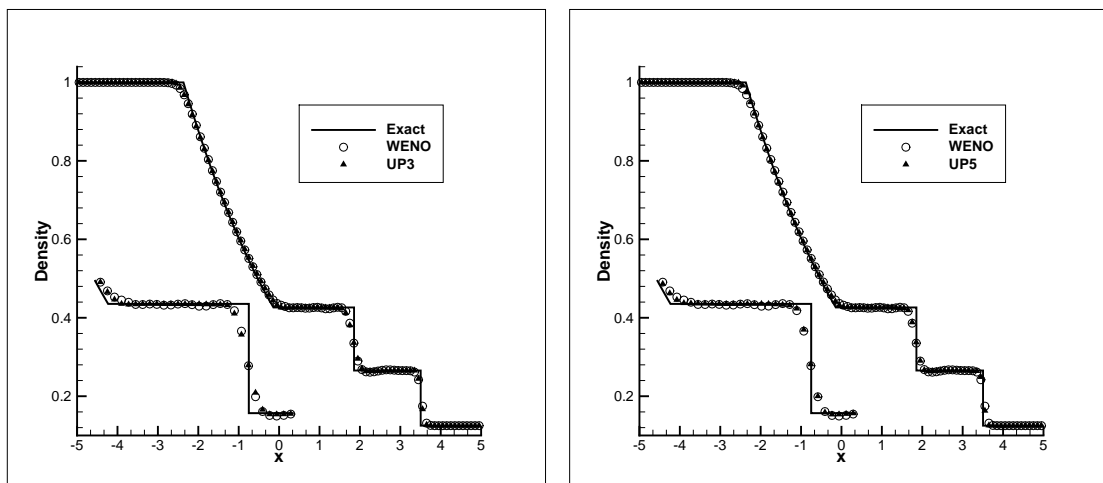


Figure 3: Density profiles of solutions to the Sod problem obtained by the second type of schemes: left: UP3; right: UP5.

Now we see the density result at $t = 2$ in Figs. 2-4 which also show the details on the computational zone $[0,2]$. Note that in the right figure of Fig. 2, the results by the current WENO-like scheme appear a little oscillation. Here the results are different from that in original references [26, 27]. As we mentioned in Section 3.3, it is mainly because the current implement of WENO is in a much simplified way compared with the traditional method with respect to both the implementation strategy (especially without the characteristic decomposition) and the quadrature strategy. The hybrid superbee scheme reduces the oscillations around the contact discontinuity and the hybrid WENO

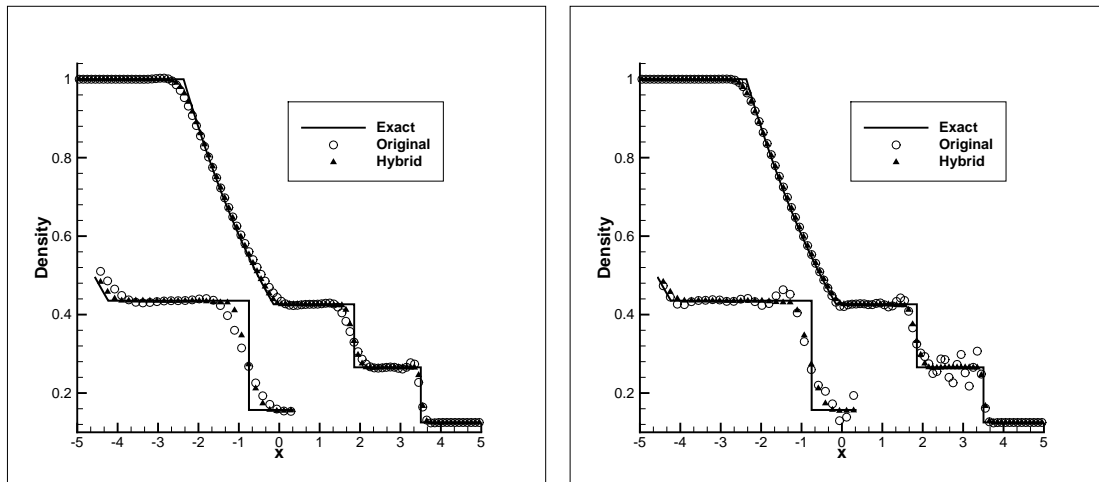


Figure 4: Density profiles of solutions to the Sod problem obtained by the third type of schemes: left: hybrid schemes compared with original method with $k^{(2)}=0.3$, $k^{(4)}=0.03$; right: hybrid schemes compared with original method with $k^{(2)}=0.05$, $k^{(4)}=0.008$.

scheme obtains the completely oscillation-free solution profile. The second type of hybrid schemes also achieve oscillation-free characteristic and the accuracy of UP3/UP5 is comparable/superior to current WENO-like scheme, see for example the details around $x = -2.4$, $x = -0.1$, $x = 1.8$ and $x = 3.5$. For the central scheme, the performance of the method is obviously improved by the hybridization. We see the hybrid central scheme succeeds in both the stabilization of the discontinuities and the preservation of the low diffusion.

4.3 Blast-wave interaction

In order to examine the robustness across strong shock waves, the interaction of blast waves [23] is considered. The computational domain is $[0,1]$ with 400 zones and the initial conditions are

$$(\rho, u, p) = \begin{cases} 1, 0, 1000, & 0.0 < x < 0.1, \\ 1, 0, 0.01, & 0.1 < x < 0.9, \\ 1, 0, 100, & 0.9 < x < 1.0. \end{cases} \quad (4.2)$$

The computation is stopped at $t = 0.038$. Density results are given in Figs. 5-9, where the exact solution is obtained with a finer grid solution of 2000 points. Figs. 5-9 also show the details on the extrema and the discontinuities. Again the reason of oscillatory results with the WENO-like scheme is due to the much simplified implementation of current WENO method. In authors' opinion, it may be both the implementation strategy (in particular without the characteristic decomposition) and the quadrature strategy that have caused oscillatory results of the WENO-like scheme for this demanding test problem.

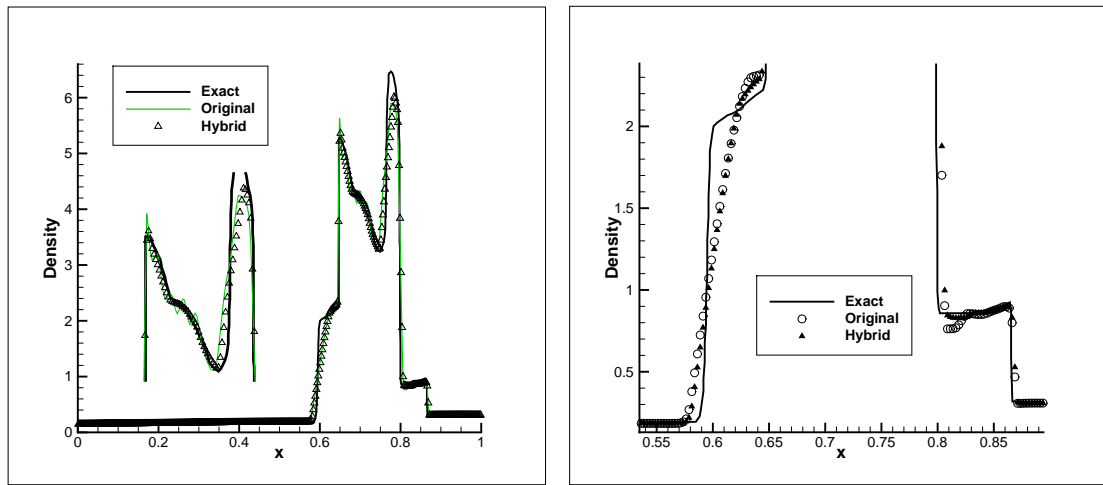


Figure 5: Density profiles of solutions to the blast-wave interaction obtained by the hybrid and original superbee schemes, left: global solution with close view on the extrema; right: local details around discontinuities at $x=0.6$ and $x=0.85$.

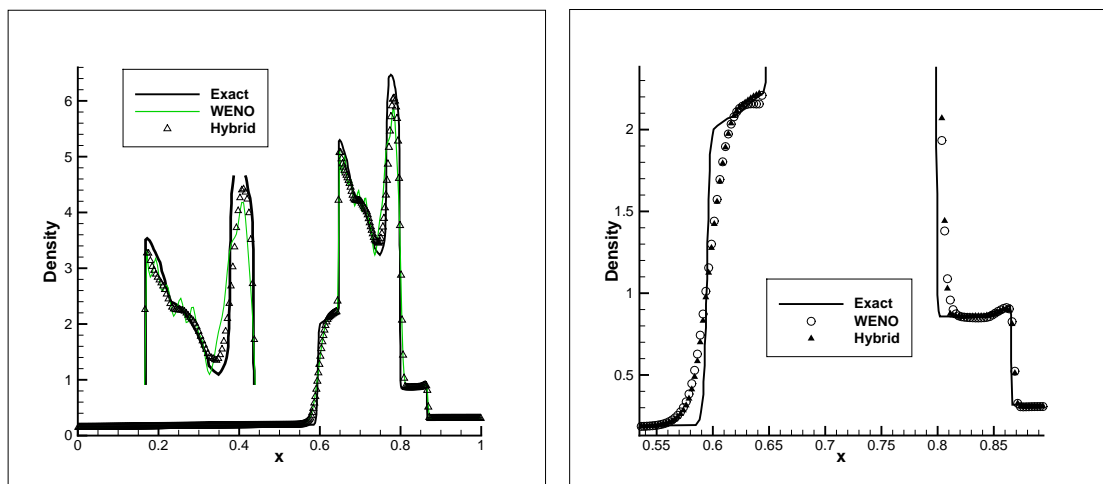


Figure 6: Density profiles of solutions to the blast-wave interaction obtained by WENO-like scheme with and without hybridization left: global solution with close view on the extrema; right: local details around discontinuities at $x=0.6$ and $x=0.85$.

And it is also noted that the original central scheme with $k^{(2)} = 0.05$, $k^{(4)} = 0.008$ fails to converge. Again the hybrid schemes are compared with the corresponding methods as described in Subsection 4.2. Several observations can be obtained through the comparison. First, the hybrid schemes eliminate all types of oscillations effectively. Second, the accuracy of smooth extrema and the resolution of shock and contact discontinuities are well preserved and even improved after the hybridization. Third, the hybrid UP5 scheme has achieved the most accurate simulation of smooth flow structures as well as the high-

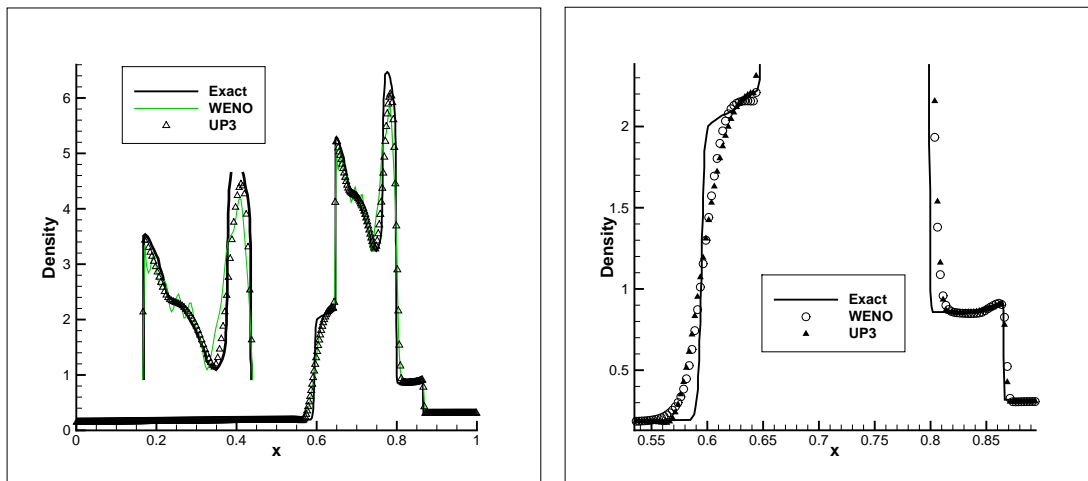


Figure 7: Density profiles of solutions to the blast-wave interaction obtained by the hybrid UP3 and WENO-like without hybridization, left: global solution with close view on the extrema; right: local details around discontinuities at $x=0.6$ and $x=0.85$.

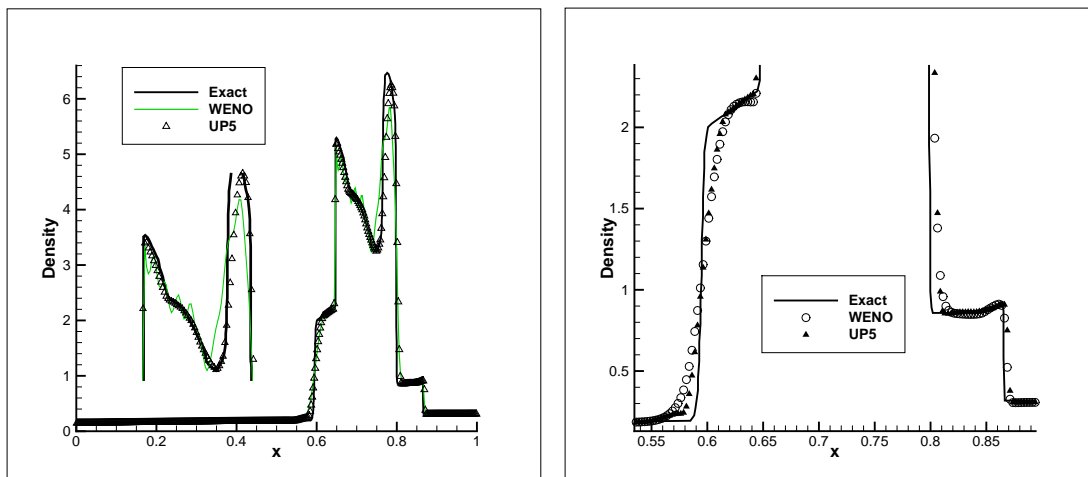


Figure 8: Density profiles of solutions to the blast-wave interaction obtained by the hybrid UP5 and WENO-like without hybridization, left: global solution with close view on the extrema; right: local details around discontinuities at $x=0.6$ and $x=0.85$.

est resolution around the discontinuities. And the hybrid central scheme also captures the fine flow details including the shock at $x=0.87$ though the scheme shows a little more dissipative on the contact discontinuities when compared with upwind schemes.

4.4 Double Mach reflection

An incident shock $Ma = 10$ past a 30° wedge, a well-known test case [23], is performed on meshes with the edge length equal to $1/480$. The density contour at $t=0.2$ is shown in

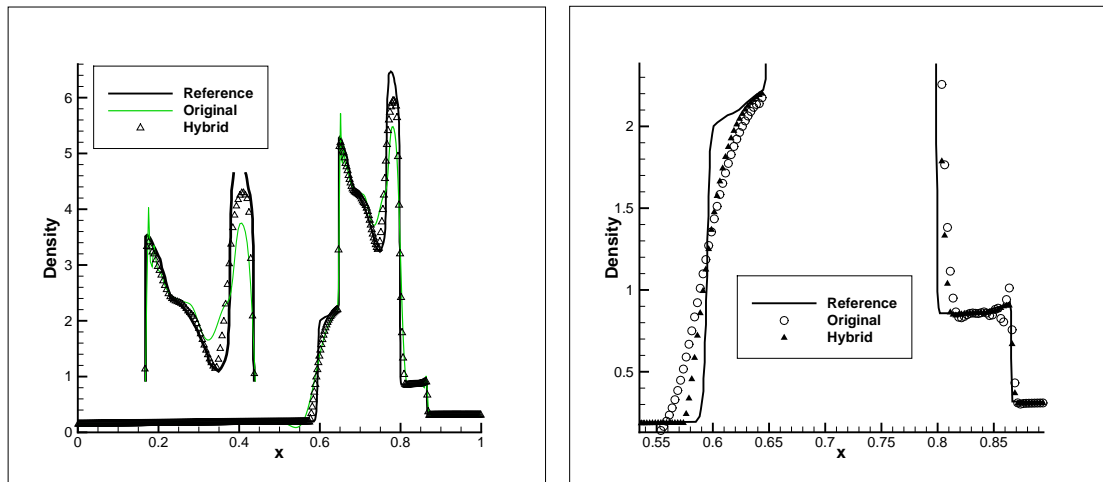


Figure 9: Density profiles of solutions to the blast-wave interaction obtained by the third type of schemes compared with the original central scheme with parameters $k^{(2)}=0.3$, $k^{(4)}=0.03$, left: global solution with close view on the extrema; right: local details around discontinuities at $x=0.6$ and $x=0.85$.

Fig. 10 and the "zoomed-in" figures around the double Mach stem obtained by different schemes, are given in Figs. 11-13. All the figures are showing 30 equally spaced contour lines from 2 to 22.

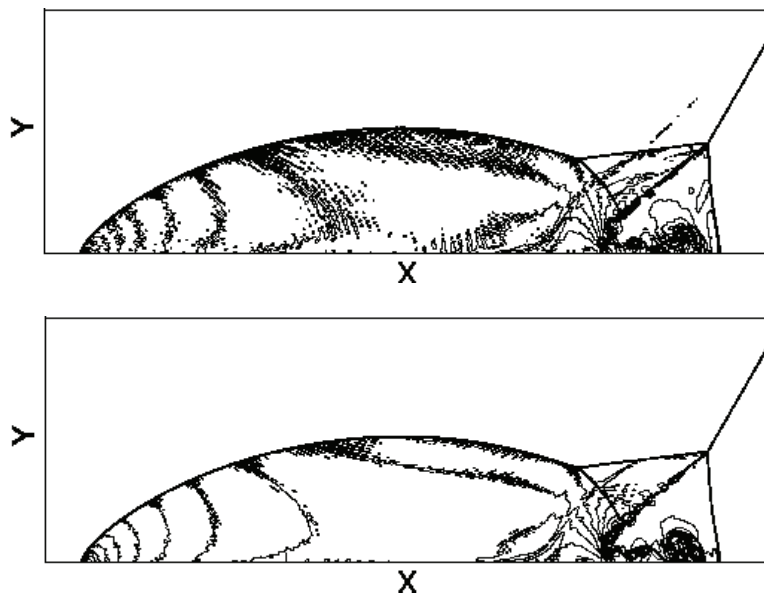


Figure 10: Double Mach reflection problem: density contour, top: original superbbee scheme; bottom: hybrid superbbee scheme.

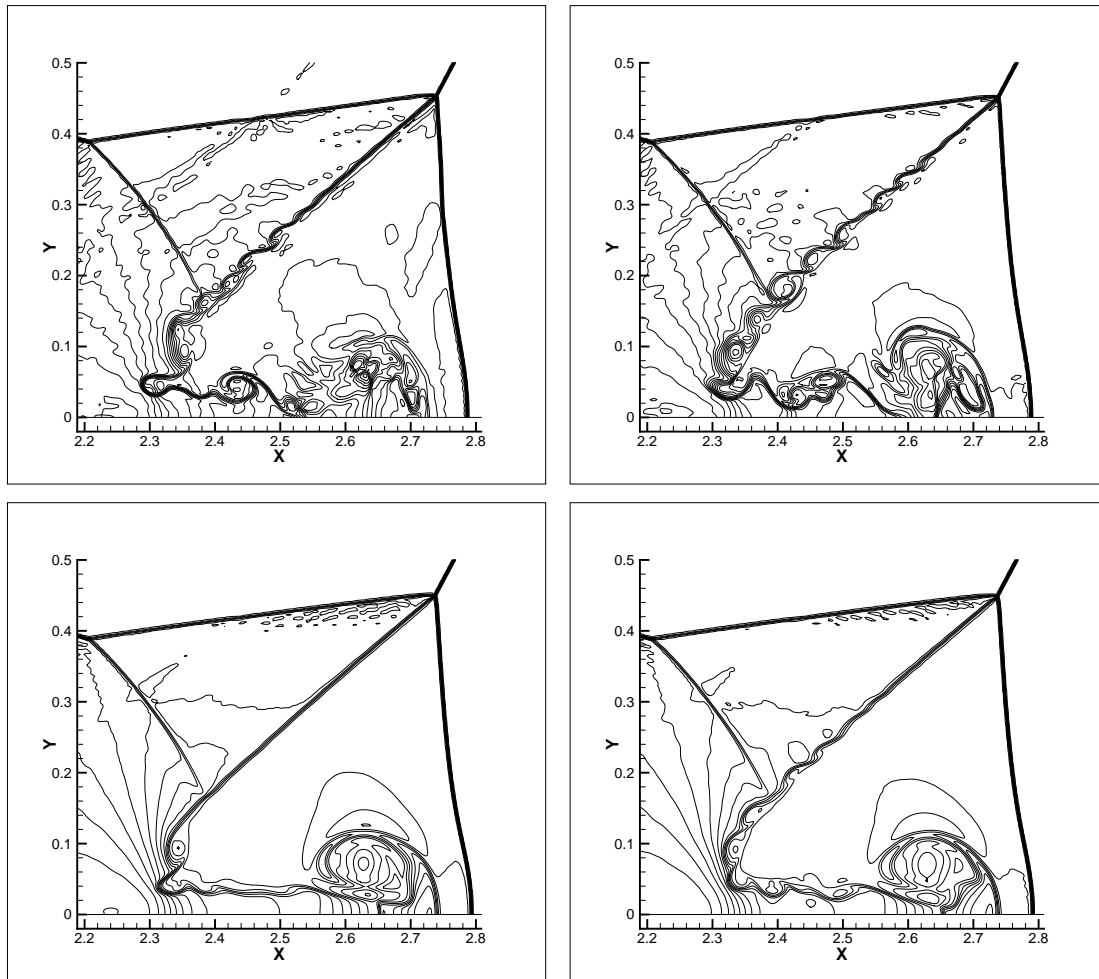


Figure 11: Double Mach reflection problem obtained by the first type of schemes: zoom-in pictures around the Mach stem left: original schemes; right: hybrid schemes; top: superbee schemes; bottom: WENO-like schemes.

Fig. 10 clearly displays the performance of original superbee method can be much improved by hybridizing shock-capturing scheme. Not only have the oscillations around the shocks but also the unphysical fluctuations at smooth flow zone been significantly reduced by the hybrid scheme. As illustrated by Figs. 11-13, hybrid schemes are indeed able to capture shock and small delicate structures of the blow-up region around the double Mach stems fairly well. In Fig. 11 the hybridization even makes WENO scheme capture more flow details. And this result is also consistent with our research conclusion in [8], which is a carefully designed TVD scheme can show better resolution than a fifth-order WENO scheme. In Fig. 12, we again observe the accuracy of UP3/UP5 is comparable/superior to current WENO-like scheme method. In Fig. 13, where the original central scheme with $k^{(2)} = 0.05$, $k^{(4)} = 0.008$ diverges, the hybrid central scheme outper-

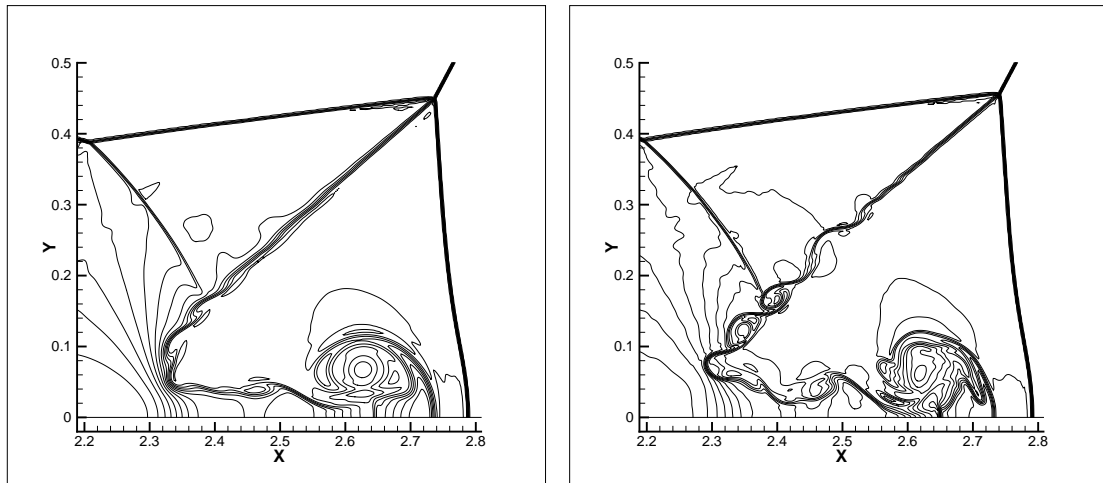


Figure 12: Double Mach reflection problem obtained by the second type of schemes: zoom-in pictures around the Mach stem left: hybrid UP3 scheme; right: hybrid UP5 scheme.

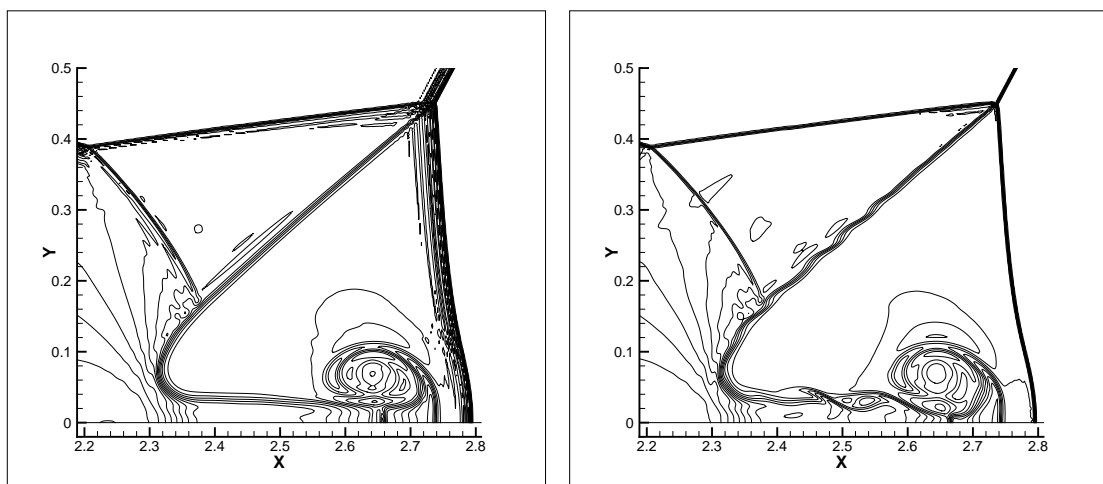


Figure 13: Double Mach reflection problem obtained by the third type of schemes: zoom-in pictures around the Mach stem left: original central scheme with $k^{(2)}=0.3$, $k^{(4)}=0.03$; right: hybrid central scheme.

forms the original one in both aspects of the shock-capturing and complex flows simulation. In Fig. 14 we show some of the plots of hybrid schemes about the cells that fail to fulfill detection criterion. One can see the identified cells are on the whole around the shocks and it is also expected that for the first type of hybrid schemes fewer cells have been identified because either the superbee or the current WENO-like scheme in itself has possessed more capability of stabilizing the discontinuities when compared to linear upwind reconstruction or central method with a low dissipation/dispersion.

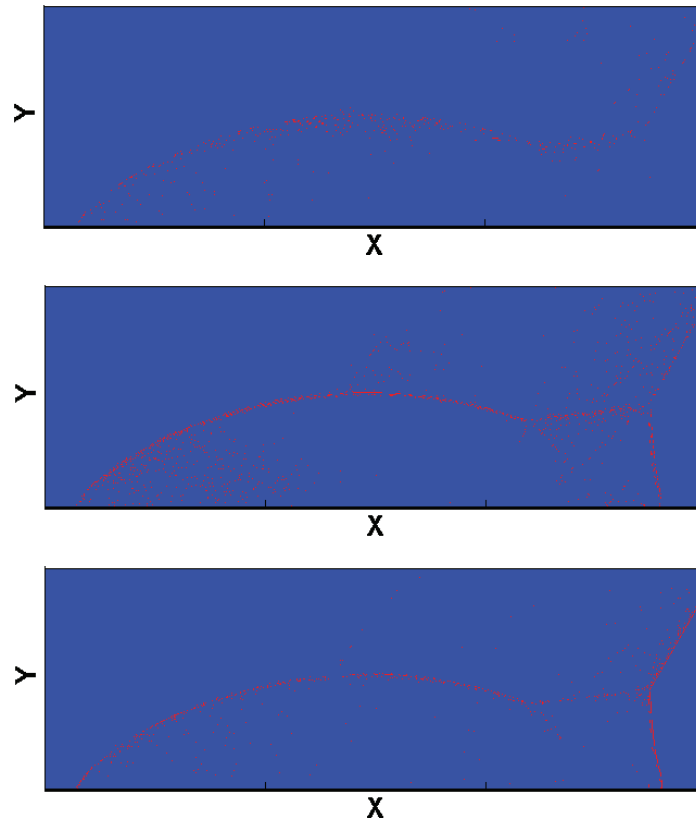


Figure 14: Double Mach reflection problem: cells that fail to fulfill detection criterion are shown in red top: the first type of scheme, hybrid WENO; middle: the second type of scheme, hybrid UP5; bottom: the third type of scheme.

4.5 A Mach 3 wind tunnel with a step

The problem under consideration is a Mach 3 flow in a wind tunnel with a step. The tunnel is 1 length unit high and 3 length units long. The step is 0.2 length units high and is located at 0.6 length units from the left-hand end of the tunnel. The boundary conditions are that of a reflecting surface along the walls of the tunnel, and inflow/outflow boundary conditions are applied at the inlet and exit. The numerical experiment is performed on a grid consisting of two structured blocks with an element size of $1/320$. Figs. 15-17 show the density contours computed by three types of schemes at time $t=4$ with 30 equally spaced contour lines from 0.32 to 6.15. And Fig. 18 gives some of the plots of hybrid schemes about the cells that fail to fulfill detection criterion.

For the first type of schemes, again strongly oscillatory solutions are obtained by the original superbee method while more smooth and appropriate results are achieved by the hybrid method. At the meantime the current WENO-like method fails to converge

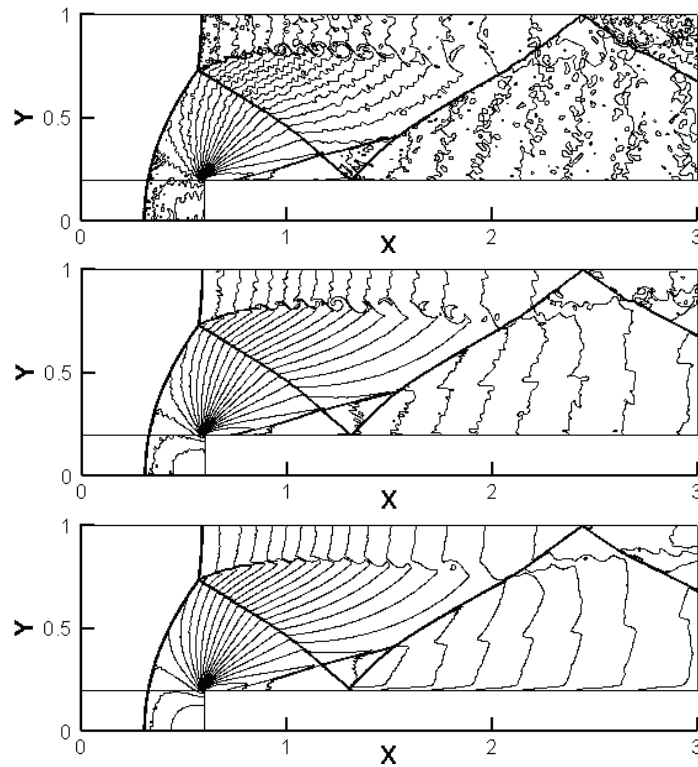


Figure 15: Density contours for the Mach 3 wind tunnel with a step problem obtained by the first type of schemes top: original superbbee scheme; middle: hybrid superbbee scheme; bottom: hybrid WENO scheme.

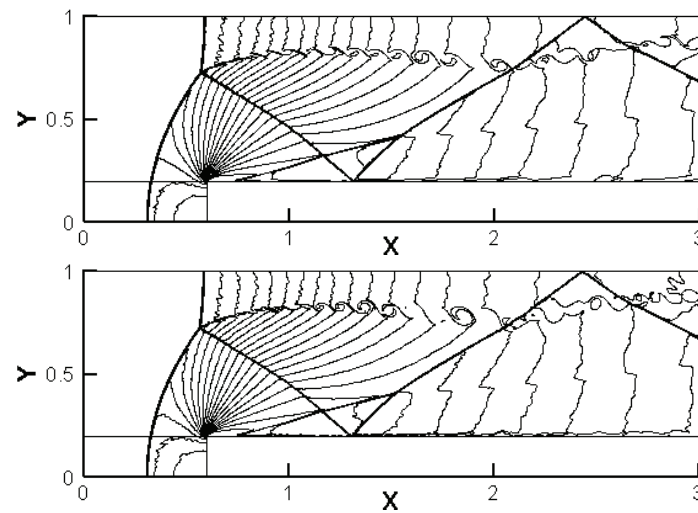


Figure 16: Density contours for the Mach 3 wind tunnel with a step problem obtained by the second type of schemes top: hybrid UP3 scheme; bottom: hybrid UP5 scheme.

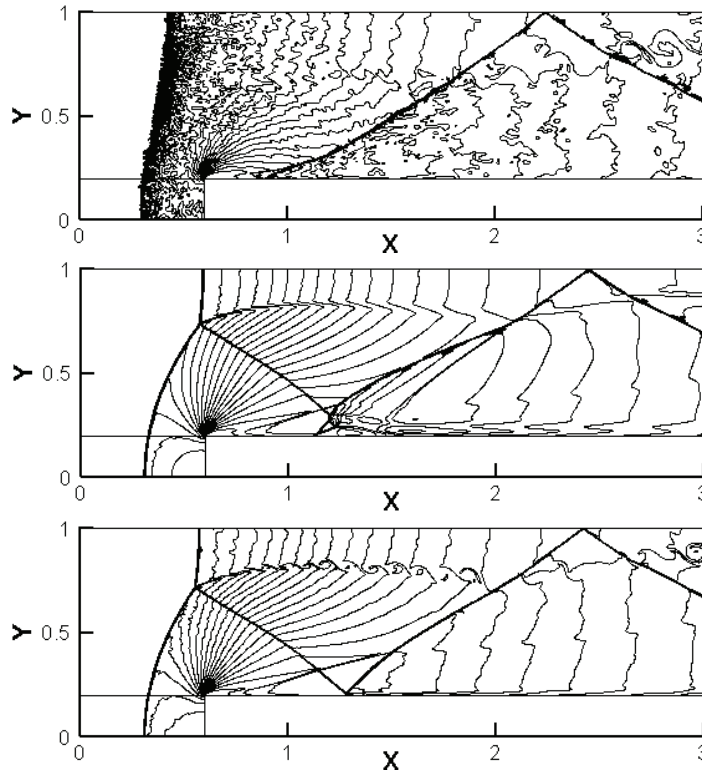


Figure 17: Density contours for the Mach 3 wind tunnel with a step problem obtained by the third type of schemes top: original method with $k^{(2)}=0.05$, $k^{(4)}=0.008$; middle: original method with $k^{(2)}=0.3$, $k^{(4)}=0.03$; bottom: hybrid method.

for this case while the hybrid one achieves accurate numerical prediction, demonstrating the robustness enhancement due to the hybridization. For the second type of hybrid schemes, the UP3 and UP5 methods gain oscillation-free solutions, and compared with current WENO-like scheme, they improve the resolution of the upper slip line from the triple point, especially for the resolution of the physical instability and rollup of the contact line. For the third type of schemes, the original method with the $k^{(2)}=0.05$, $k^{(4)}=0.008$, though it has not blown up the simulation, gives unacceptable results. And for the original method with the $k^{(2)}=0.3$, $k^{(4)}=0.03$, the singularity of the corner leads to an erroneous entropy layer as well as a spurious solution at the bottom wall. However, no spurious results are observed for hybrid methods, and the accuracy for the upper slip line and the resolution for various shock structures have also been improved. From Fig. 18 we see the detection criterion detects the cells where the solutions are recomputed by more robust characteristic-based MUSCL scheme. The identified cells are on the whole around those strong discontinuities and again fewer cells have been identified by the first type of hybrid schemes when compared to the second and third type of hybrid schemes.

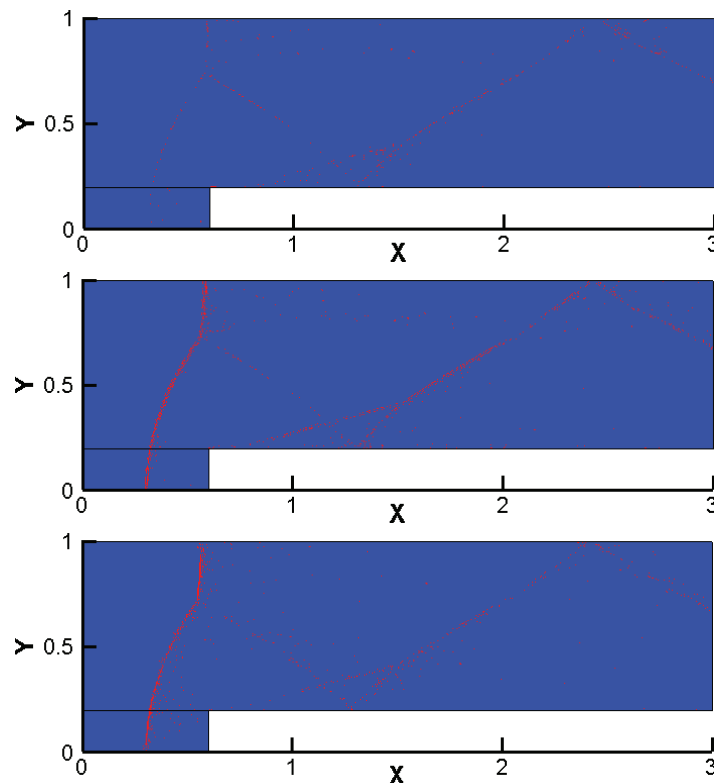


Figure 18: A Mach 3 wind tunnel with a step problem: cells that fail to fulfill detection criterion are shown in red top: the first type of scheme, hybrid WENO; middle: the second type of scheme, hybrid UP5; bottom: the third type of scheme.

4.6 Transonic flow past a NACA0012 airfoil

We consider inviscid transonic flow past a NACA0012 airfoil configuration with $Ma=0.8$, the angle of attack 1.25° . The mesh used in the computation is shown in Fig. 19. An O-type meshing strategy consists of 100 points along the upper and lower surfaces of the airfoil and 45 points in the direction normal to the surface. This case has been selected to test the designed schemes on block-structured body-fitted grids. Figs. 20-22 present the computed pressure coefficient distributions obtained by the original and hybrid methods. Again in the right figure of Fig. 20, the oscillation with the WENO-like scheme is believed to be caused by the simplified implementation of current WENO method. As can be seen, the hybrid schemes are indeed able to eliminate the spurious oscillations in the vicinity of shocks, especially for the original central scheme with the set of parameters of $k^{(2)}=0.05$, $k^{(4)}=0.008$. In Fig. 21, we can observe the accuracy of UP3/UP5 is comparable/superior to current WENO-like method. And it seems that the hybrid UP5 scheme has the best resolution for both the shocks on the upper and the lower surface.

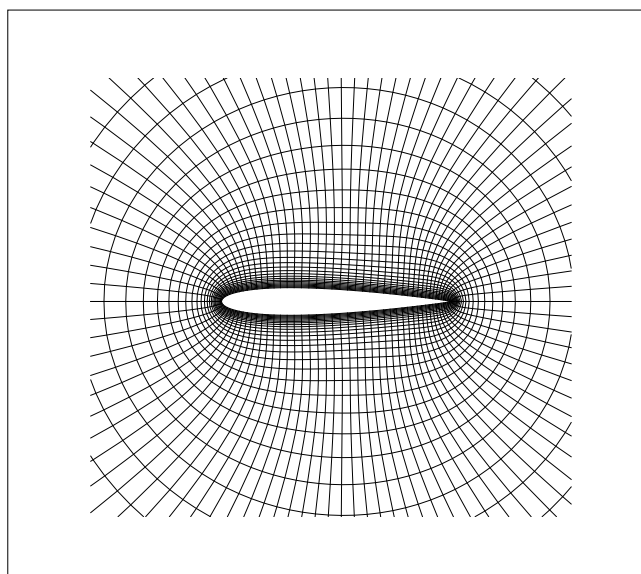


Figure 19: NACA0012 airfoil mesh zoom in.

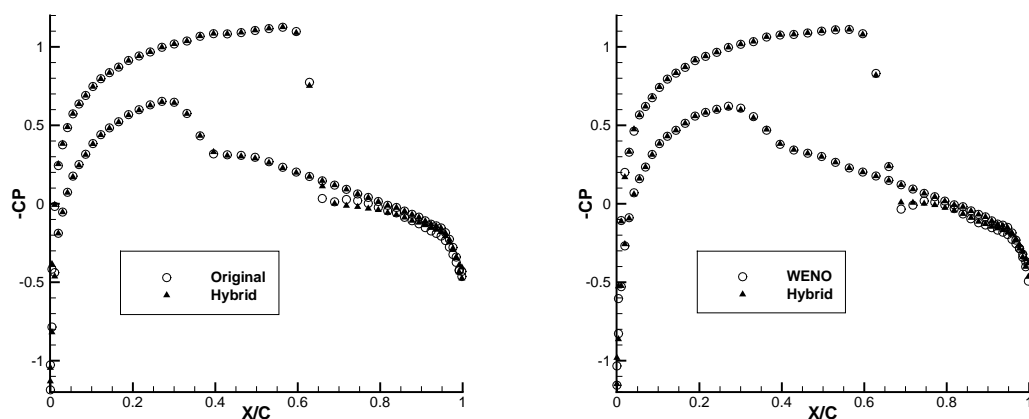


Figure 20: Pressure distributions for the transonic flow past a NACA0012 airfoil problem obtained by the first type of schemes left: hybrid superbee compared with original method; right: current WENO-like with and without hybridization.

4.7 3D explosion problem

To validate the hybrid schemes in three spatial dimensions, we solve an explosion problem [24] on the computational domain $[1:1] \times [1:1] \times [1:1]$. The initial condition consists of two regions of constant but different values of gas parameters separated by a sphere

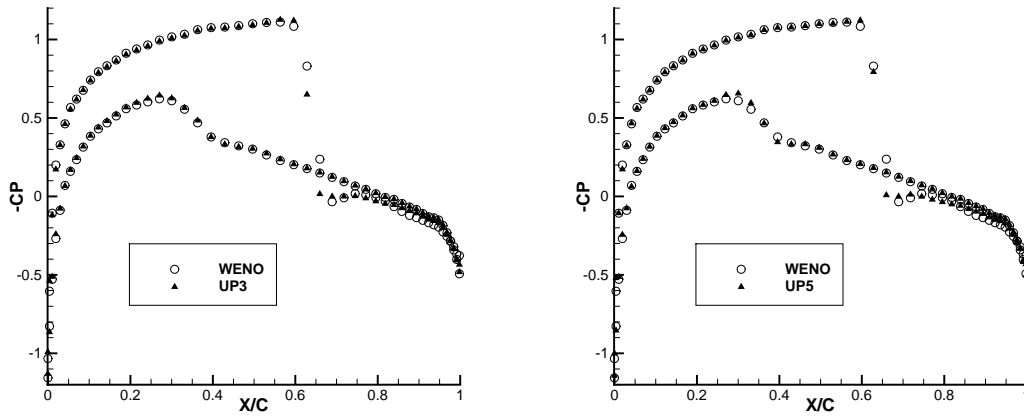


Figure 21: Pressure distributions for the transonic flow past a NACA0012 airfoil problem obtained by the second type of schemes left: hybrid UP3 compared with WENO-like without hybridization; right: hybrid UP5 compared with WENO-like without hybridization.

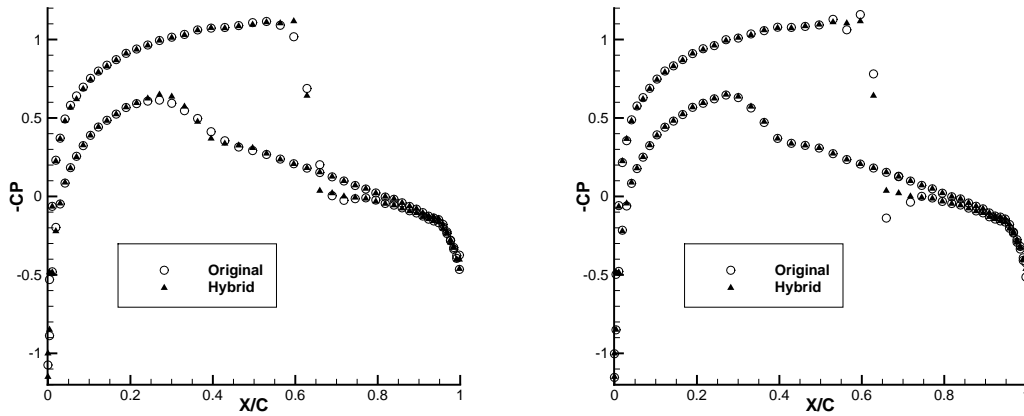


Figure 22: Pressure distributions for the transonic flow past a NACA0012 airfoil problem obtained by the third type of schemes left: hybrid scheme compared with original method with $k^{(2)}=0.3, k^{(4)}=0.03$; right: hybrid scheme compared with original method with $k^{(2)}=0.05, k^{(4)}=0.008$.

of radius 0.4:

$$(\rho, p) = \begin{cases} (1.0, 1.0), & r \leq 0.4, \\ (0.125, 0.1), & r > 0.4, \end{cases} \quad u, v, w = 0, \quad r = \sqrt{x^2 + y^2 + z^2}. \quad (4.3)$$

The numerical solution is computed at the output time $t=0.25$ on a mesh of 400 cells in each coordinate direction and the results of the hybrid and original schemes are compared with a reference radial solution, which is obtained by solving the one-dimensional

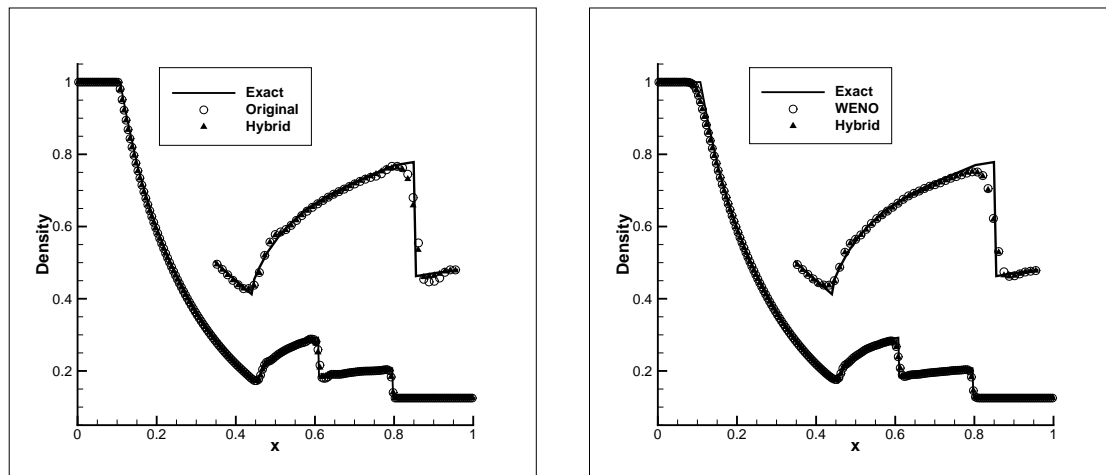


Figure 23: Density results to the 3D explosion problem obtained by the first type of schemes: left: superbee; right: WENO-like.

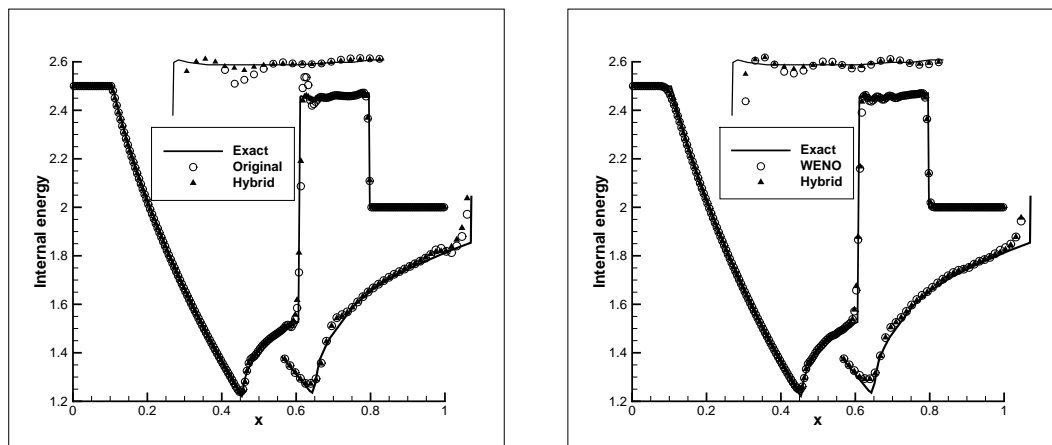


Figure 24: Internal energy results to the 3D explosion problem obtained by the first type of schemes: left: superbee; right: WENO-like.

Euler equations with a geometric source term on a very fine mesh [24]. We present distributions of gas density and internal energy in Figs. 23-28, where zoom-in pictures around discontinuities or extrema are also provided. From Figs. 23-24 one can see the over/undershoots about the discontinuity at $x = 0.6$ have been suppressed by the hybrid methods, meantime the accuracy on the extrema and the resolution on the shock and contact discontinuity have not been compromised with reference to the original methods. One could also compare results of the superbee and current WENO-like schemes and find that the 2nd-order scheme even has higher resolution on the extrema at $x = 0.1$ and $x = 0.45$ and higher resolution on the contact discontinuity at $x = 0.6$. For the second

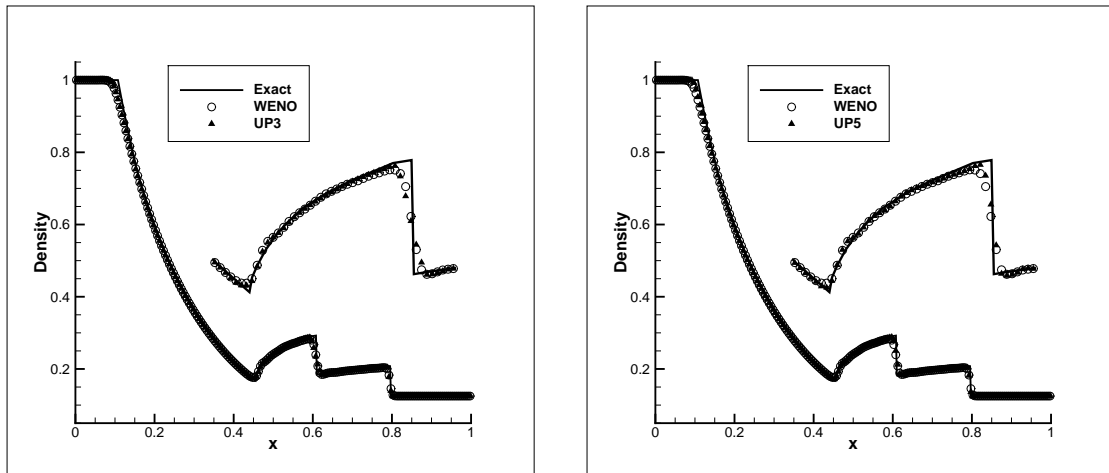


Figure 25: Density results to the 3D explosion problem obtained by the second type of schemes: left: UP3; right: UP5.

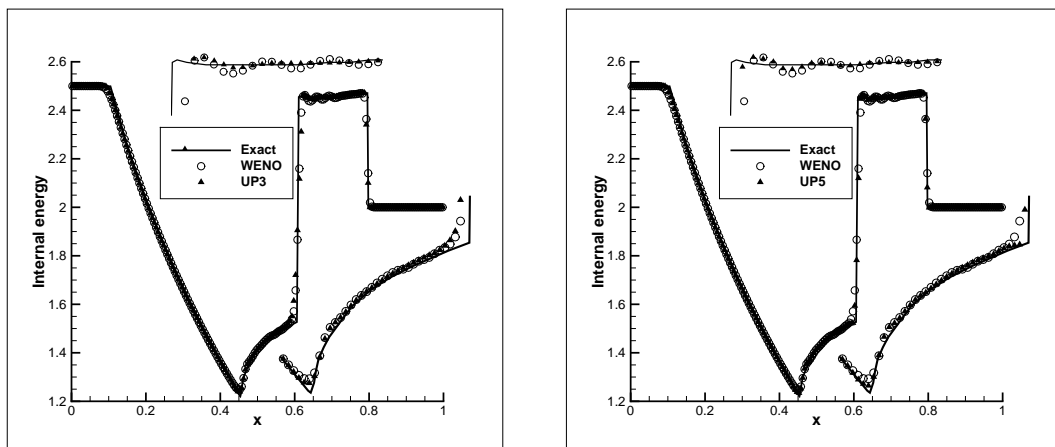


Figure 26: Internal energy results to the 3D explosion problem obtained by the second type of schemes: left: UP3; right: UP5.

type of hybrid schemes, the resolution of extrema and discontinuities are both improved as the order of accuracy of the scheme increased. And compared with current WENO-like without hybridization, less oscillation is obtained by the hybrid schemes. As for the central schemes, it seems that the original methods are inclined to produce oscillatory solutions before the discontinuity. The hybrid scheme has removed almost all the oscillations and has achieved more accurate prediction for the smooth zone, see for example the zoom-in results of $[0.6, 0.8]$ from Fig. 28. Note that zoom-in results of $[0.6, 0.8]$ are not shown for the right figure in Fig. 28 since the oscillation is quite obvious for the original method.

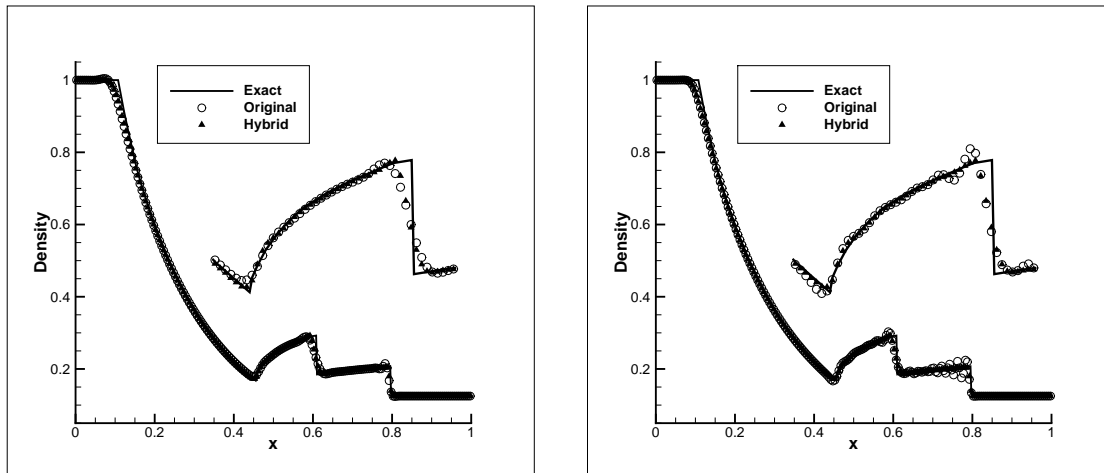


Figure 27: Density results to the 3D explosion problem obtained by the third type of schemes: left: hybrid schemes compared with original method with $k^{(2)}=0.3$, $k^{(4)}=0.03$; right: hybrid schemes compared with original method with $k^{(2)}=0.05$, $k^{(4)}=0.008$.

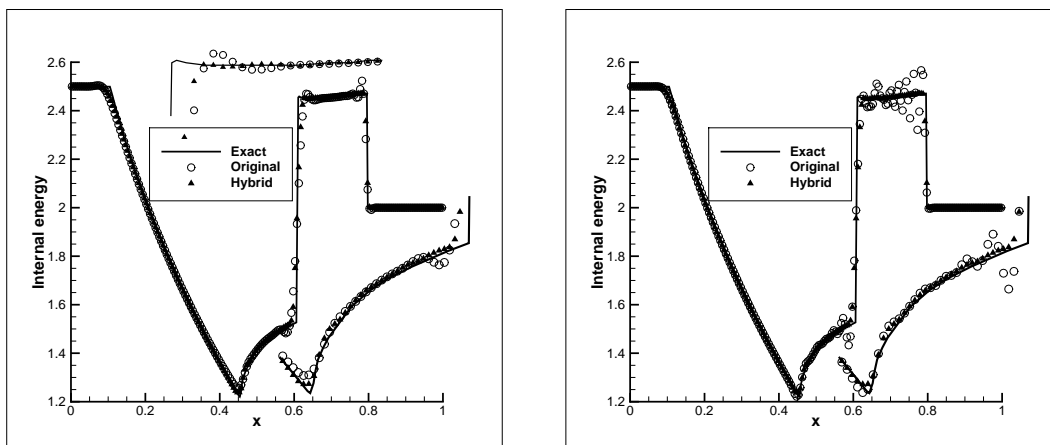


Figure 28: Internal energy results to the 3D explosion problem obtained by the third type of schemes: left: hybrid schemes compared with original method with $k^{(2)}=0.3$, $k^{(4)}=0.03$; right: hybrid schemes compared with original method with $k^{(2)}=0.05$, $k^{(4)}=0.008$.

4.8 Further discussion on the efficiency of hybrid schemes

In this subsection, the results of computational time comparison between the hybrid schemes and original methods are shown in Table 1, where the CPU times of different schemes have been normalized with original superbee scheme in each test case. One can see that the hybrid schemes do increase the computational cost in comparison with their corresponding methods and Table 1 shows that the first type of hybrid scheme requires 30%–40% CPU time more than the corresponding methods while for the third type of hy-

Table 1: Comparison on the normalized CPU time of different schemes for double Mach reflection, a Mach 3 wind tunnel with a step and 3D explosion problem.

Cases	CPU time (normalized with original superbee scheme)							
	original superbee	hybrid superbee	WENO-like without hybridization	hybrid WENO	hybrid UP3	hybrid UP5	original central	hybrid central
double Mach reflection	1.0	1.40	1.26	1.74	1.47	1.58	0.71	1.18
a Mach 3 wind tunnel with a step	1.0	1.42	—	1.76	1.48	1.59	0.72	1.20
3D explosion	1.0	1.36	1.27	1.71	1.44	1.54	0.71	1.16

brid scheme, the increase of computing cost is about 60%–70% compared with original central scheme. On the other hand, it is also notable from the table that the hybrid central scheme is more efficient than the WENO-like without hybridization. In fact due to small computational cost of central scheme, the third type of hybrid scheme is the most efficient one in all present hybrid schemes, which can make this scheme an efficient and favorable hybrid strategy, especially for the problems containing both discontinuities and complicated flow structures. However it should be noted that the increased computational cost can vary with different cases. And it is hoped that the results provided here can be used in choosing the “optimal” scheme when one considers both the CPU time and the quality of the results.

5 Conclusion

In this paper, a general framework for designing various types of hybrid schemes is established based on the concept of MOOD method. The idea is to take advantage of the MOOD and turn the construction of hybrid schemes into the construction of different numerical flux for the interface of the cells. The methodology utilizes low dissipation or dispersion but less robust schemes to update the solution and then implements robust and high resolution schemes to deal with problematic situations. Three types of hybrid schemes, built upon MUSCL/WENO reconstruction, linear reconstruction and central scheme respectively, have been developed in the present framework. And a characteristic-based MUSCL scheme is employed as the shock-capturing method. Classical test cases for solving the Euler system are performed to examine the accuracy, the resolution and non-oscillatory property of the designed hybrid schemes. The numerical experiments demonstrate that the hybrid schemes eliminate all types of oscillations effectively while maintaining or improving the resolution for both the discontinuous and smooth flow features. We also show the performance of original methods can be significantly improved due to the proposed hybridization and some results by the 2nd-order and 3rd-order schemes are even comparable to those obtained by current WENO-like scheme.

Further work will be carried out including the extension of current hybrid schemes to achieve more desirable mathematical properties such as DMP property and/or positivity-preserving property. A possible way to preserve the positivity is to use the self-

adjusting positivity preserving scheme [25] instead of the current characteristic MUSCL in the present framework. Another possible way to ensure positivity-preserving or DMP property would be to add more loop with a more dissipative TVD scheme or even a first order Godunov-type scheme being used for the cells that fail to provide an acceptable solution according to the MOOD detection criteria after applying characteristic-based MUSCL scheme [18].

References

- [1] S. Clain, S. Diot and R. Loubère, A high-order finite volume method for systems of conservation laws multi-dimensional optimal order detection (MOOD), *J. Comput. Phys.*, 230(10) (2011), 4028-4050.
- [2] B. van Leer, Towards the ultimate conservation difference scheme V: A second-order sequel to Godunov's method, *J. Comput. Phys.*, 32(1) (1979), 101-136.
- [3] X. D. Liu, S. Osher and T. Chan, Weighted essentially non-oscillatory schemes, *J. Comput. Phys.*, 115 (1994), 200-212.
- [4] G. Jiang and C. W. Shu, Efficient implementation of weighted ENO schemes, *J. Comput. Phys.*, 126(1) (1996), 202-228.
- [5] A. Jameson, W. Schmidt and E. Turkel, Numerical solution of the Euler equations by finite volume methods using Runge-Kutta time-stepping schemes, AIAA-1981-1259, 1981.
- [6] C. Le Touze et al., Multislope MUSCL method for general unstructured meshes, *J. Comput. Phys.* (2014), <http://dx.doi.org/10.1016/j.jcp.2014.12.032>
- [7] D. Balsara and C. W. Shu, Monotonicity preserving weighted essentially non-oscillatory schemes with increasingly high order of accuracy, *J. Comput. Phys.*, 160 (2000), 405-452.
- [8] J. Yu, C. Yan and Z. Jiang, A hybrid high resolution low dissipation scheme for compressible flows, *Chinese Journal of Aeronautics*, 24 (2011), 417-424.
- [9] N. A. Adams and K. Shariff, A high-resolution hybrid compact-ENO scheme for shock-turbulence interaction problems, *J. Comput. Phys.*, 127 (1996), 27-46.
- [10] S. Pirozzoli, Conservative hybrid compact-WENO schemes for shock-turbulence interaction, *J. Comput. Phys.*, 178 (2002), 81-117.
- [11] Y. Ren, M. Liu and H. Zhang, A characteristic-wise hybrid compact-WENO scheme for solving hyperbolic conservation laws, *J. Comput. Phys.*, 192 (2003), 365-386.
- [12] D. J. Hill and D. I. Pullin, Hybrid tuned center-difference-WENO method for large eddy simulations in the presence of strong shocks, *J. Comput. Phys.*, 194 (2004), 435-450.
- [13] B. Cosat and W. S. Don, High order hybrid central-WENO finite difference scheme for conservation laws, *J. Comput. Appl. Math.*, 204 (2007), 209-218.
- [14] G. Li and J. Qiu, Hybrid weighted essentially non-oscillatory schemes with different indicators, *J. Comput. Phys.*, 229 (2010), 8105-8129.
- [15] S. Diot, S. Clain and R. Loubère, Improved detection criteria for the multi-dimensional optimal order detection (MOOD) on unstructured meshes with very high-order polynomials, *Comput. Fluids*, 64 (2012), 43-63.
- [16] S. Diot, R. Loubère and S. Clain, The MOOD method in the three-dimensional case: very-high-order finite volume method for hyperbolic systems, *Int. J. Numer. Meth. Fluids*, 73 (2013), 362-392.
- [17] R. Loubère, M. Dumbser and S. Diot, A new family of high order unstructured MOOD and ADER finite volume schemes for multidimensional systems of hyperbolic conservation

- laws, Commun. Comput. Phys., 16 (2014), 718-763.
- [18] M. Dumbser, O. Zanotti, R. Loubère and S. Diot, A posteriori subcell limiting of the discontinuous Galerkin finite element method for hyperbolic conservation laws, J. Comput. Phys., 278 (2014), 47-75.
 - [19] J. Yu and C. Yan, On the performance of two shock-capturing schemes, Journal of Beijing University of Aeronautics and Astronautics, 36(1) (2010), 10-13.
 - [20] P. L. Roe, Approximate Riemann solvers, parameter vectors, and difference schemes, J. Comput. Phys., 43 (1981), 357-372.
 - [21] W. J. Rider, Methods for extending high-resolution schemes to non-linear systems of hyperbolic conservation laws, Int. J. Numer. Meth. Fluids, 17(10) (1993), 861-885.
 - [22] R. H. Nichols, R. W. Tramel and P. G. Buning, Evaluation of two high-order weighted essentially nonoscillatory schemes, AIAA J., 46(12) (2008), 3090-3102.
 - [23] P. Woodward and P. Colella, Numerical simulation of two-dimensional fluid flows with strong shocks, J. Comput. Phys., 54 (1984), 115-173.
 - [24] E. F. Toro, Riemann Solvers and Numerical Methods for Fluid Dynamics, second ed., Springer Berlin, 1999.
 - [25] D. S. Balsara, Self-adjusting, positivity preserving high order schemes for hydrodynamics and magnetohydrodynamics, J. Comput. Phys., 231 (2012), 7504-7517.
 - [26] V. Titarev and E. Toro, Finite-volume WENO schemes for three-dimensional conservation laws, J. Comput. Phys., 201 (2004), 238-260.
 - [27] C. W. Shu, High order weighted essentially nonoscillatory schemes for convection dominated problems, SIAM Review, 51(1) (2009), 82-126.